

Ballistic transport of long wavelength phonons and thermal conductivity accumulation in nanograined silicon-germanium alloys

Long Chen, Jeffrey L. Braun, Brian F. Donovan, Patrick E. Hopkins, and S. Joseph Poon

Citation: *Appl. Phys. Lett.* **111**, 131902 (2017); doi: 10.1063/1.4986884

View online: <http://dx.doi.org/10.1063/1.4986884>

View Table of Contents: <http://aip.scitation.org/toc/apl/111/13>

Published by the [American Institute of Physics](#)

The banner features a dark blue background with a network of glowing yellow and white nodes connected by thin blue lines, creating a complex web-like structure. The text is overlaid on the left side of this network.

SciLight

Sharp, quick summaries **illuminating**
the latest physics research

Sign up for **FREE!**

AIP
Publishing

Ballistic transport of long wavelength phonons and thermal conductivity accumulation in nanograined silicon-germanium alloys

Long Chen,¹ Jeffrey L. Braun,² Brian F. Donovan,^{2,a)} Patrick E. Hopkins,^{1,2,3,b)} and S. Joseph Poon^{1,c)}

¹Department of Physics, University of Virginia, Charlottesville, Virginia 22904-4714, USA

²Department of Mechanical & Aerospace Engineering, University of Virginia, Charlottesville, Virginia 22904-4746, USA

³Department of Materials Science and Engineering, University of Virginia, Charlottesville, Virginia 22904-4745, USA

(Received 7 June 2017; accepted 9 September 2017; published online 27 September 2017)

Computationally efficient modeling of the thermal conductivity of materials is crucial to thorough experimental planning and theoretical understanding of thermal properties. We present a modeling approach in this work that utilizes a frequency-dependent effective medium theory to calculate the lattice thermal conductivity of nanostructured solids. This method accurately predicts a significant reduction in the experimentally measured thermal conductivity of nanostructured Si₈₀Ge₂₀ systems reported in this work, along with previously reported thermal conductivities in nanowires and nanoparticles in matrix materials. We use our model to gain insights into the role of long wavelength phonons on the thermal conductivity of nanograined silicon-germanium alloys. Through thermal conductivity accumulation calculations with our modified effective medium model, we show that phonons with wavelengths much greater than the average grain size will not be impacted by grain boundary scattering, counter to the traditionally assumed notion that grain boundaries in solids will act as diffusive interfaces that will limit long wavelength phonon transport. This is further supported by using time-domain thermorefectance at different pump modulation frequencies to measure the thermal conductivity of a series nanograined silicon-germanium alloys. *Published by AIP Publishing.* [<http://dx.doi.org/10.1063/1.4986884>]

The conflict between growing demands for energy and limited non-renewable energy sources has attracted great interest over the past few decades, which has spurred a multitude of researchers to explore clean and renewable energy. Thermoelectric (TE) materials, which can generate electricity from waste heat, could play an important role in a global sustainable energy solution. The performance of a thermoelectric material is evaluated by a dimensionless figure of merit ZT , which is equal to $S^2\sigma T/\kappa$, where S is the Seebeck coefficient, σ is the electrical conductivity, and κ is the thermal conductivity. Among the TE materials, silicon-germanium structures continue to be the main focus of tremendous investment due to their widespread integration in TE power generation, optoelectronic devices, and high-mobility transistors. In these materials, it has been shown that the thermal conductivity, κ , can be decreased while preserving the electronic power factor, and thus, the figure of merit ZT is increased at much lower cost.¹

To simulate the lattice thermal conductivity of materials and nanosystems, several approaches have been advanced in the literature, including the Callaway-based model^{2,3} derived from the Boltzmann Transport Equation (BTE),⁴⁻⁸ Monte Carlo simulations with varying phonon frequency dependences,⁹ and various methods to calculate the phonon mean free path (MFP) distributions, including analytical models,¹⁰⁻¹² numerical results from molecular dynamics (MD)

simulations,¹³⁻¹⁷ and first-principles calculations based on the density functional theory.¹⁸⁻²³ Notably, Minnich and Chen used an Effective Medium Approach (EMA) to predict the thermal conductivity of heterogeneous nanostructures and modified the phonon mean free paths in both matrix materials and nanoparticles.²⁴ This modification came from assuming phonon single particle scattering of embedded nano-inclusions and incorporating a thermal boundary resistance at the nano-inclusion/matrix interface. However, this method is only applicable in small volume fractions of embedded particles since it is based on the first-order T-matrix approximation.

In this current work, we revisit the use of the MFP spectrum in nanocomposites and upgrade the effective medium approach^{25,26} to include a phonon wavelength dependence (i.e., non-gray approach) in deriving the expressions for the lattice thermal conductivity of a bulk system; we then extend this derivation to their fully nanostructured states. We use our model to gain insights into the role of long wavelength phonons on the thermal conductivity of nanograined silicon-germanium alloys via time domain thermorefectance (TDTR) measurements of the frequency dependence in thermal conductivity.^{27,28} Through thermal conductivity accumulation calculations with our modified effective medium model, we show that phonons with wavelengths much greater than the average grain size will not be impacted by grain boundary scattering, counter to the traditionally assumed notion that grain boundaries in solids will act as diffusive interfaces that will limit long wavelength phonon transport.

To develop our model, we start with the phonon Boltzmann transport equation:

^{a)}Current Address: Department of Physics, United States Naval Academy, Annapolis, Maryland 21402-5002, USA

^{b)}phopkins@virginia.edu

^{c)}sjp9x@virginia.edu

$$\frac{\partial N_{q\lambda}}{\partial t} + \vec{v}_{q\lambda} \cdot \nabla N_{q\lambda} + \vec{F} \cdot \nabla_v N_{q\lambda} = \left(\frac{\partial N_{q\lambda}}{\partial t} \right)_c, \quad (1)$$

where $N_{q\lambda}$ is the phonon distribution with wavenumber q , in phonon branch λ , $\vec{v}_{q\lambda}$ is the phonon group velocity, \vec{F} is an external force, and $\left(\frac{\partial N_{q\lambda}}{\partial t} \right)_c$ is the time rate of change in the phonon distribution due to collisions. The fundamental assumptions of this work are as follows: all of the parameters in Eq. (1) are phonon frequency dependent, the system is in steady state $\frac{\partial N_{q\lambda}}{\partial t} = 0$, and there is no external force. Thus, under the time relaxation approximation, we can derive heat flux in wave vector space as

$$\vec{J} = -\sum_{\lambda} \iiint \hbar \omega_{q\lambda} \left(\vec{v}_{q\lambda} \cdot \nabla T \frac{\partial n_{q\lambda}}{\partial T} \tau_{q\lambda} \right) \vec{v}_{q\lambda} dq_i dq_j dq_k. \quad (2)$$

Comparing this with $\vec{J} = -\kappa \nabla T$, we can write κ in q space as

$$\kappa = \sum_{\lambda} \iiint \hbar \omega_{q\lambda} \frac{\partial n_{q\lambda}}{\partial T} \tau_{q\lambda} (v_{q\lambda})^2 dq_i dq_j dq_k. \quad (3)$$

To determine the scalar form of the thermal conductivity, the spectral heat capacity and the tensor form of the thermal conductivity derived above are compared with $\kappa(q) = \frac{1}{3} C(q) v(q) L(q)$, where $L(q)$ is the mean free path. The spectral thermal conductivity for a given wavenumber q can be written as

$$\kappa(q) = \frac{D}{(2\pi)^3} 4\pi q^2 \sum_{\lambda} \hbar \omega_{q\lambda} \frac{\partial n_{q\lambda}}{\partial T} (v_{q\lambda})^2 \tau_{q\lambda}, \quad (4)$$

where we use D as a normalization factor which is used to preserve the number of phonon modes of the system. We determine D by equating the experimental specific heat to the value predicted from our calculations. The total phonon scattering time is determined by contributions from defect scattering, Umklapp scattering, and grain boundary scattering, and the forms of these scattering times and additional assumptions are outlined in the [supplementary material](#). Modeling the thermal conductivity of nanomaterials with the use of a fixed length scale, l , for boundary scattering, such as a film thickness or grain size, is common in the literature and assumes that all phonons with mean free paths greater than l will scatter at this boundary and have a limited contribution to heat transport compared to their bulk counterparts. We refer to this as the ‘‘Fixed Boundary Length’’ (FBL) model.

Moving beyond the FBL, it is important to account for the physical geometry of the structure that creates the boundary that could impede phonon transport. For example, the geometry, characteristic structure, and properties of the material that are creating the boundaries must also be accounted for in thermal conductivity calculations. Thus, we can consider boundary scattering, l , as the characteristic length of the material and defined as $l = (\rho * \sigma)^{-1}$, where ρ is the number of particles in a unit volume and σ is the cross section. We can further break down σ as the combination of scattering cross sections in two extreme regimes:²⁹

$$\sigma_{\text{total}}^{-1} = \sigma_{\text{Ray}}^{-1} + \sigma_{\text{nGeo}}^{-1}, \quad (5)$$

where σ_{Ray} and σ_{nGeo} are scattering cross sections in the Rayleigh limit and near geometric limit, respectively. Kim and Majumdar proposed an approximate analytical solution to estimate the phonon scattering cross section of polydispersed spherical nanoparticles,²⁹ which we adopt in our model calculations here and detail in the [supplementary material](#). We refer to our model calculations using $l = (\rho * \sigma)^{-1}$ with Eq. (5) as the ‘‘Spectral Boundary Length’’ (SBL) model.

Finally, following Nan *et al.*^{25,26} to extend our simulation to nanostructured systems, the differential effective medium approach (DEM) was applied. The advantage of the DEM approach is that it uses pre-determined parameters when compared to other nearly parameter free methods. In addition, the modified term in the DEM already accounts for the lower order inter-particle phonon scattering, which yields an easier and more efficient way to calculate lattice thermal conductivity. To apply the DEM, Poon *et al.* reformulated what Bruggeman developed from a physical standpoint and interpreted the results in terms of higher-order (multi-particle) scattering.^{30,31} The key point is that at volume fraction ϕ , the thermal conductivity of the matrix is updated to $\kappa(\phi)$. Previously, $d\phi$ was substituted by an effective $d\phi' = d\phi / (1 - \phi)$, where $1 - \phi$ is the volume of the unoccupied host. By doing this, a small volume fraction of particles is incrementally added to the matrix. After each addition, the host is updated, and the added particle scatters phonons in the updated matrix, which gives rise to the multi-particle effect. Upon addition of the particles in the matrix up to a particle volume fraction, ϕ , approaching 100%, we achieve the lattice thermal conductivity of a specific phonon with wavenumber q . This can be expressed as

$$\kappa(q) = \frac{\kappa_p(q)}{1 + \frac{\alpha_{p0}(q) * \kappa_p(q)}{\kappa_{p0}(q)}}, \quad (6)$$

where $\kappa_p(q)$ is the thermal conductivity of embedded nanoparticles with wavenumber q , $\kappa_{p0}(q)$ is the intrinsic lattice thermal conductivity of the particle material in a bulk form, and $\alpha_{p0} = R_{p0} \kappa_{p0} / (d/2)$, which is the thermal resistance parameter, where R_{p0} is the thermal boundary resistance estimated as $R_{p0} \approx 8 / (C_{p0} v_{p0})$.²⁴ We refer to this model as the ‘‘DEM’’ model; more details of this model are provided in the [supplementary material](#).

To validate our model, we compare our calculations with the measured thermal conductivity of silicon nanowires by Li *et al.*³² As shown in Fig. 1(a), our model can also capture the thermal conductivity reduction in Si nanowires due to boundary scattering, similar to more traditional phonon-transport models based on semi-classical formalisms, as summarized by Yang and Dames.³³ We also calculate the thermal conductivity of Si-Ge nanocomposites ($d = 10$ nm Si nanoparticles in a Ge bulk matrix) and compare these calculations with various previous models in Fig. 1(b). Our non-gray DEM simulation results in more rapid reductions in the thermal conductivity as a function of the volume fraction at low volume fractions as compared to Minnich’s gray and non-gray EMA models.²⁴ Also, our non-gray DEM results agree well with Jeng’s Monte Carlo

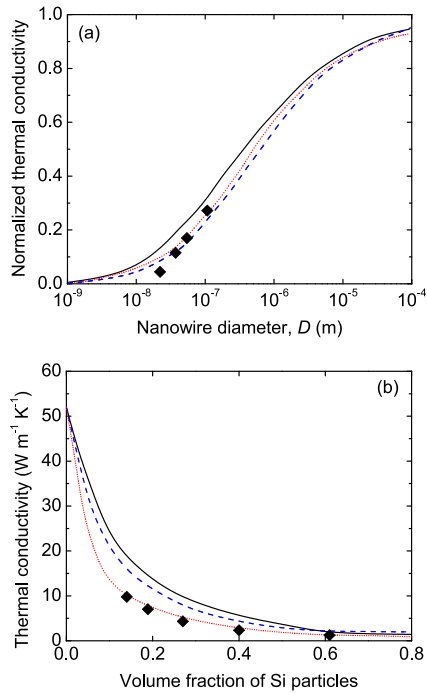


FIG. 1. (a) Normalized thermal conductivity of silicon nanowires calculated using the Holland model (solid black) and BvKS model (dashed, blue), both of which were taken from the study by Yang and Dames,³³ as compared to our non-gray DEM (dotted red), and the experimental data from the study by Li *et al.*³² (b) Lattice thermal conductivity κ_L of the Si/Ge nanocomposite dependence on Si nanoparticles's volume fraction at room temperature ($T = 300 \text{ K}$), with an average grain size $d = 10 \text{ nm}$. Non-gray DEM simulation with the grain size dispersion-standard deviation of $0.577d$ (dotted, red) is compared with Jeng's MC simulation (black diamonds),³⁴ gray EMA (black solid), and non-gray EMA (blue dashed).

(MC) simulations,³⁴ which are supported by experimental results.^{34,35} In addition, Ordonex-Miranda *et al.* showed that the DEM model and the finite element method were consistent with each other in their thermal conductivity study.³⁶

Considering the results shown in Figs. 1(a) and 1(b) together, the use of our modified DEM in our method for phonon thermal conductivity predictions yields an easier, more efficient, and more accurate way to calculate the lattice thermal conductivity of both homo- and heterogeneous nanomaterials and nanocomposites as compared to previously used approaches. Therefore, our proposed model can be used to study phonon transport in nanocomposite systems going beyond simple thermal conductivity predictions via calculations of phonon thermal conductivity accumulation as a function of the mean free path.

In the remainder of this work, we extend the use of our DEM approach to nanograined Si-Ge bulk systems. We fabricate a silicon control sample and $\text{Si}_{80}\text{Ge}_{20}$ samples with varying grain sizes. Ingots of both compositions are prepared by arc melting under an argon atmosphere. Ingots are pulverized into $1\text{--}30 \mu\text{m}$ size powders. These micro powders are consolidated using Spark Plasma Sintering (Thermal Technologies SPS 10-4). To produce fully dense compacted disks with relative large grain sizes, Si and $\text{Si}_{80}\text{Ge}_{20}$ samples are sintered at 1280°C and 1210°C , respectively, for 4 min under 60 MPa. As for the nanostructured systems $\text{Si}_{80}\text{Ge}_{20}$, micro-powders of Si and $\text{Si}_{80}\text{Ge}_{20}$ are loaded into a 440C stainless steel vial and two $0.5''$ and four $0.25''$ stainless steel balls. This process is

performed in a glove box under an argon atmosphere. The vial is then sealed and placed in a SPEX 8000D vibrational mixer. The powders are ball milled for 40 h for the $\text{Si}_{80}\text{Ge}_{20}$ systems. The ball milled powders are then compacted by SPS. We determine the grain size of the disks by the cleaved cross section analyzed under a SEM (Fig. 2). The grain sizes for the silicon control extend to as large as $30 \mu\text{m}$, while the ranges of grain sizes determined for the various $\text{Si}_{80}\text{Ge}_{20}$ samples are listed in the caption of Fig. 2. We mechanically polish all samples after deposition to facilitate TDTR measurements, and the resulting RMS roughnesses determined via mechanical profilometry maps were $30 \pm 10 \text{ nm}$.

We conduct experimental measurements of the thermal conductivity of these systems using TDTR with varying pump modulation frequencies, which effectively varies the heater length scale. This approach has been recently vetted for studying accumulation effects on the thermal conductivity of alloys.³⁷ The fabrication and characterization of the various Si and $\text{Si}_{80}\text{Ge}_{20}$ samples and details of our TDTR measurements, including the validity of the use of a diffusive heat equation-based model for TDTR data analysis,³⁷ are included in the [supplementary material](#).

We alter the modulation frequency of the pump beam during our TDTR measurements from 1.49 MHz to 12.2 MHz . The thermal penetration depth (L_e) was determined using the solution to the radially symmetric heat diffusion equation where the full spatial temperature profile was calculated.³⁸ The use of our relatively large pump and probe spot sizes allows our TDTR measurements at the various frequencies to be directly related to the thermal transport physics in the cross-plane direction, therefore reducing measurement sensitivities to in-plane non-diffusive thermal transport.^{37,39} Furthermore, the use of Al as our thin film transducer will allow for direct comparison of our measurements to previous reports of Fourier failure in Si-Ge-based systems without the potential for additional electron-phonon resistances in the metal film to complicate our results and analyses.⁴⁰

As discussed by several recent works,^{37,40–44} we relate the changing thermal penetration depth with the varying frequencies during TDTR experiments to changes in the net heat flux. Thus, we modify our EMA modeling approach to separate the thermal conductivity of the samples into a high frequency mode component (diffusive) and a low frequency mode component (quasi-ballistic). To determine the cut-off MFP that separates these high and low frequency mode regimes, a plausible way is to equate the MFP to the thermal penetration depth, and then, this MFP is used to determine the corresponding wavenumber q . As another approach, we also use a compact heat conduction model based on the two-fluid assumption (bridge function).⁴⁴ In this model, we write the net heat flux in the form of $J = j^{LF} + j^{HF}$, where j^{LF} and j^{HF} are the low and high frequency mode contributions to the

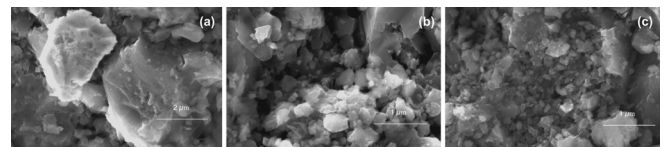


FIG. 2. SEM micrographs of $\text{Si}_{80}\text{Ge}_{20}$ systems: (a) $\text{Si}_{80}\text{Ge}_{20}$ $2.0 \pm 0.17 \mu\text{m}$, (b) $\text{Si}_{80}\text{Ge}_{20}$ $110 \pm 21 \text{ nm}$, and (c) $\text{Si}_{80}\text{Ge}_{20}$ $73 \pm 29 \text{ nm}$.

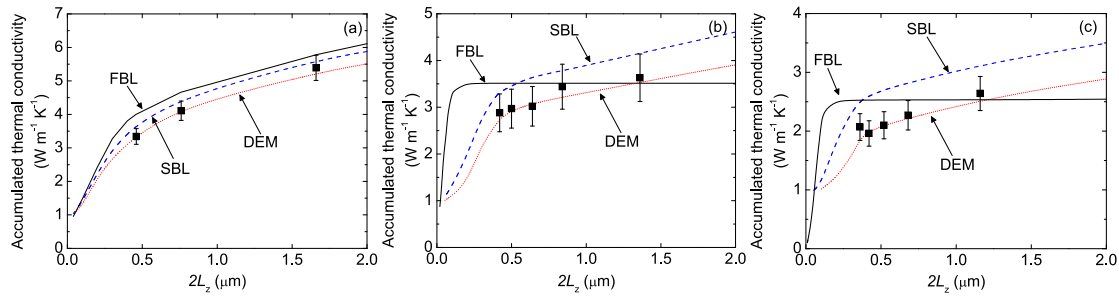


FIG. 3. Modeled (lines) and measured (points) accumulated thermal conductivity vs. thermal penetration depth for $\text{Si}_{80}\text{Ge}_{20}$ samples with average grain sizes of (a) $2\ \mu\text{m}$, (b) $110\ \text{nm}$, and (c) $73\ \text{nm}$. Note, we define the TDTR penetration depth as $2L_z$, as we discuss in the [supplementary material](#).

heat flux. This approach is detailed in the [supplementary material](#). We find that for these alloys, both approaches yield similar results due to the alloy transport being dominated by the near-zone center modes.

We now use our approach to analyze the TDTR data taken on the $\text{Si}_{80}\text{Ge}_{20}$ systems, comprised of samples with average grain sizes of $2\ \mu\text{m}$, $110\ \text{nm}$, and $73\ \text{nm}$. For all nano-grained samples, we observe the frequency dependence in the measured thermal conductivity, as shown in Fig. 3, implying that as our measurement depth is increased, the thermal conductivity is also increased. Note that these data show similar trends to the previously reported frequency dependent TDTR data on SiGe alloys.^{37,45,46} We attribute this effect to the accumulation of the lattice thermal conductivity as we probe into the length scales that capture the heat carrying mean free paths in this system. Based on previous works, this frequency dependent trend might suggest that phonons with mean free paths greater than the thermal penetration depth carry substantial amounts of heat in these systems, and our measurements are related to an accumulation of phonon mean free paths.^{37,40–44} This, however, is counter-intuitive to traditionally implemented phonon transport dynamics that assume phonons with mean free paths greater than the grain size will scatter and thus not contribute to thermal conductivity (as predicted via the traditionally assumed FBL model).

The traditionally implemented assumptions in the FBL model force all phonons to scatter at a length scale defined by the grain boundary. Thus, regardless of the assumption of what phonons are considered quasi-ballistic and diffusive (i.e., hard cutoff or bridge function to separate these two regimes), the FBL always predicts a leveling off of the accumulative thermal conductivity at much shorter length scales than that observed in the experimental data (Fig. 3), since by definition, it restricts the propagation of long wavelength phonons. The use of the bridge function and implementation of the two-fluid assumption in the modeling of the accumulation of thermal conductivity yields predicted trends, in good agreement with our measured frequency dependent thermal conductivity data. For the three different grain sizes, our DEM approach exhibits improved agreement with the experimental data over the varying thermal penetration depths as compared to the other models (FBL and SBL). Thus, the spectral contribution to thermal conductivity in the nano-grained $\text{Si}_{80}\text{Ge}_{20}$ samples cannot be predicted from traditionally assumed boundary scattering models (e.g., FBL, which will truncate phonon transport at a limiting length scale, such as a grain boundary). Phonon scattering cross sections,

such as those calculated when applying the SBL and DEM, must be accounted for to properly model this phenomenon.

The FBL fails to account for the long wavelength phonon transport, as it assumes that these phonons will scatter with the grain boundaries. This discrepancy is most pronounced for the 110 and $73\ \text{nm}$ samples. While long wavelength-dominated phonon transport is well known in crystalline alloys (due to high frequency phonon-mass impurity scattering),^{47–50} the role of grain boundaries and their interplay among long wavelength phonon transport and phonon-mass impurity scattering has been less-frequently explored. Our results suggest that creating nanograins in crystalline alloys may not have as pronounced an effect on lowering thermal conductivity as predicted by traditional boundary scattering theories, such as those assumed in the FBL. Since the majority of the thermal transport in crystalline alloys is driven by the long wavelength, large wave vector phonons (cf. Fig. 3), the scattering cross section of nanograins could be too small to create a significant impact on the majority of the heat carrying phonons, which is demonstrated by the modest frequency dependence in the 110 and $73\ \text{nm}$ alloys as compared to the $2\ \mu\text{m}$ sample.

In summary, we present a modeling approach that utilizes a frequency-dependent effective medium method to calculate the lattice thermal conductivity of nanostructured solids. This allows for the study of spectral phonon scattering and spectral contributions to thermal conductivity in nanostructured solids. Through thermal conductivity accumulation calculations with our modified effective medium model, we show that phonons with wavelengths much greater than the average grain size will not be impacted by grain boundary scattering, counter to the traditionally assumed notion that grain boundaries in solids will act as diffusive interfaces that will limit long wavelength phonon transport.

See [supplementary material](#) for more details on the following: S1, Details of the “Fixed Boundary Length” (FBL) and “Spectral Boundary Length” (SBL) models, assumptions, and calculations; S2, TDTR Measurements; S3, Validity of the use of a diffusive heat equation-based model when analyzing TDTR data; S4, The cut-off mean free path vs thermal penetration depth determined by the bridge function and hard cutoff approaches; S5, Details of spectral thermal conductivity calculations using the DEM approach for nano-grained $\text{Si}_{80}\text{Ge}_{20}$ systems.

This material is based upon work supported by the Air Force Office of Scientific Research under Award No. FA9550-15-1-0079.

- ¹G. Joshi, H. Lee, Y. Lan, X. Wang, G. Zhu, D. Wang, R. W. Gould, D. C. Cuff, M. Y. Tang, M. S. Dresselhaus, G. Chen, and Z. Ren, "Enhanced thermoelectric figure-of-merit in nanostructured p-type silicon germanium bulk alloys," *Nano Lett.* **8**, 4670–4674 (2008).
- ²J. Callaway, "Model for lattice thermal conductivity at low temperatures," *Phys. Rev.* **113**, 1046–1051 (1959).
- ³W. Kim, S. L. Singer, A. Majumdar, J. M. O. Zide, D. Klenov, A. C. Gossard, and S. Stemmer, "Reducing thermal conductivity of crystalline solids at high temperature using embedded nanostructures," *Nano Lett.* **8**, 2097–2099 (2008).
- ⁴R. Yang and G. Chen, "Thermal conductivity modeling of periodic two-dimensional nanocomposites," *Phys. Rev. B* **69**, 195316 (2004).
- ⁵C. Dames and G. Chen, "Theoretical phonon thermal conductivity of Si/Ge superlattice nanowires," *J. Appl. Phys.* **95**, 682–693 (2004).
- ⁶R. Yang, G. Chen, M. Laroche, and Y. Taur, "Simulation of nanoscale multidimensional transient heat conduction problems using ballistic-diffusive equations and phonon boltzmann equation," *J. Heat Transfer* **127**, 298–306 (2005).
- ⁷R. Yang, G. Chen, and M. Dresselhaus, "Thermal conductivity of simple and tubular nanowire composites in the longitudinal direction," *Phys. Rev. B* **72**, 125418 (2005).
- ⁸Z. Wang, J. E. Alaniz, W. Jang, J. E. Garay, and C. Dames, "Thermal conductivity of nanocrystalline silicon: Importance of grain size and frequency-dependent mean free paths," *Nano Lett.* **11**, 2206–2213 (2011).
- ⁹Q. Hao, G. Zhu, G. Joshi, X. Wang, A. Minnich, Z. Ren, and G. Chen, "Theoretical studies on the thermoelectric figure of merit of nanograin bulk silicon," *Appl. Phys. Lett.* **97**, 063109 (2010).
- ¹⁰J. D. Chung, A. J. H. McGaughey, and M. Kaviani, "Role of phonon dispersion in lattice thermal conductivity modeling," *J. Heat Transfer* **126**, 376–380 (2004).
- ¹¹P. E. Hopkins, L. M. Phinney, P. T. Rakich, R. H. Olsson, and I. El-Kady, "Phonon considerations in the reduction of thermal conductivity in phononic crystals," *Appl. Phys. A* **103**, 575–579 (2011).
- ¹²P. E. Hopkins, P. T. Rakich, R. H. Olsson, I. El-Kady, and L. M. Phinney, "Origin of reduction in phonon thermal conductivity of microporous solids," *Appl. Phys. Lett.* **95**, 161902 (2009).
- ¹³S. Volz and G. Chen, "Molecular dynamics simulation of thermal conductivity of silicon nanowires," *Appl. Phys. Lett.* **75**, 2056–2058 (1999).
- ¹⁴A. Giri, J. L. Braun, J. A. Tomko, and P. E. Hopkins, "Reducing the thermal conductivity of chemically ordered binary alloys below the alloy limit via the alteration of phonon dispersion relations," *Appl. Phys. Lett.* **110**, 233112 (2017).
- ¹⁵A. Giri and P. E. Hopkins, "Spectral contributions to the thermal conductivity of C60 and the fullerene derivative PCBM," *J. Phys. Chem. Lett.* **8**, 2153–2157 (2017).
- ¹⁶J. M. Larkin and A. J. H. McGaughey, "Thermal conductivity accumulation in amorphous silica and amorphous silicon," *Phys. Rev. B* **89**, 144303 (2014).
- ¹⁷A. S. Henry and G. Chen, "Spectral phonon transport properties of silicon based on molecular dynamics simulations and lattice dynamics," *J. Comput. Theor. Nanoscience* **5**, 141–152 (2008).
- ¹⁸P. Ravindran, L. Fast, P. A. Korzhavyi, B. Johansson, P. Wills, and O. Eriksson, "Density functional theory for calculation of elastic properties of orthorhombic crystals: Application to TiSi₂," *J. Appl. Phys.* **84**, 4891–4904 (1998).
- ¹⁹K. Esfarjani, G. Chen, and H. T. Stokes, "Heat transport in silicon from first-principles calculations," *Phys. Rev. B* **84**, 085204 (2011).
- ²⁰L. Lindsay, D. A. Broido, and T. L. Reinecke, "First-principles determination of ultrahigh thermal conductivity of boron arsenide: A competitor for diamond?," *Phys. Rev. Lett.* **111**, 025901 (2013).
- ²¹A. Ward and D. A. Broido, "Intrinsic phonon relaxation times from first-principles studies of the thermal conductivities of Si and Ge," *Phys. Rev. B* **81**, 085205 (2010).
- ²²A. Ward, D. A. Broido, D. Stewart, and G. Deinzer, "Ab initio theory of the lattice thermal conductivity in diamond," *Phys. Rev. B* **80**, 125203 (2009).
- ²³A. Seko, A. Togo, H. Hayashi, K. Tsuda, L. Chaput, and I. Tanaka, "Prediction of Low-thermal-conductivity compounds with first-principles anharmonic lattice-dynamics calculations and Bayesian optimization," *Phys. Rev. Lett.* **115**, 205901 (2015).
- ²⁴A. Minnich and G. Chen, "Modified effective medium formulation for the thermal conductivity of nanocomposites," *Appl. Phys. Lett.* **91**, 073105 (2007).
- ²⁵C.-W. Nan, R. Birringer, D. R. Clarke, and H. Gleiter, "Effective thermal conductivity of particulate composites with interfacial thermal resistance," *J. Appl. Phys.* **81**, 6692–6699 (1997).
- ²⁶C.-W. Nan, "Effective-medium theory of piezoelectric composites," *J. Appl. Phys.* **76**, 1155–1163 (1994).
- ²⁷D. G. Cahill, "Analysis of heat flow in layered structures for time-domain thermoreflectance," *Rev. Sci. Instrum.* **75**, 5119–5122 (2004).
- ²⁸A. J. Schmidt, "Pump-probe thermoreflectance," *Annu. Rev. Heat Transfer* **16**, 159–181 (2013).
- ²⁹W. Kim and A. Majumdar, "Phonon scattering cross section of polydispersed spherical nanoparticles," *J. Appl. Phys.* **99**, 084306 (2006).
- ³⁰S. J. Poon and K. Limtragool, "Nanostructure model of thermal conductivity for high thermoelectric performance," *J. Appl. Phys.* **110**, 114306 (2011).
- ³¹S. J. Poon, A. S. Petersen, and D. Wu, "Thermal conductivity of core-shell nanocomposites for enhancing thermoelectric performance," *Appl. Phys. Lett.* **102**, 173110 (2013).
- ³²D. Li, Y. Wu, P. Kim, L. Shi, P. Yang, and A. Majumdar, "Thermal conductivity of individual silicon nanowires," *Appl. Phys. Lett.* **83**, 2934–2936 (2003).
- ³³F. Yang and C. Dames, "Mean free path spectra as a tool to understand thermal conductivity in bulk and nanostructures," *Phys. Rev. B* **87**, 035437 (2013).
- ³⁴M.-S. Jeng, R. G. Yang, D. Song, and G. Chen, "Modeling the thermal conductivity and phonon transport in nanoparticle composites using Monte Carlo simulations," *J. Heat Transfer* **130**, 042410 (2008).
- ³⁵M. S. Dresselhaus, G. Chen, M. Y. Tang, R. G. Yang, H. Lee, D. Z. Wang, Z. F. Ren, J.-P. Fleurial, and P. Gogna, "New directions for low-dimensional thermoelectric materials," *Adv. Mater.* **19**, 1043–1053 (2007).
- ³⁶J. Ordóñez-Miranda, M. Hermens, I. Nikitin, V. G. Kouznetsova, and S. Volz, "Modeling of the effective thermal conductivity of sintered porous pastes," in *20th International Workshop on Thermal Investigations of ICs Systems Terminic* (2014), pp. 1–4.
- ³⁷R. B. Wilson and D. G. Cahill, "Anisotropic failure of Fourier theory in time-domain thermoreflectance experiments," *Nat. Commun.* **5**, 5075 (2014).
- ³⁸J. L. Braun and P. E. Hopkins, "Upper limit to the thermal penetration depth during modulated heating of multilayer thin films with pulsed and continuous wave lasers: A numerical study," *J. Appl. Phys.* **121**, 175107 (2017).
- ³⁹P. E. Hopkins, J. R. Serrano, L. M. Phinney, S. P. Kearney, T. W. Grasser, and C. T. Harris, "Criteria for cross-plane dominated thermal transport in multilayer thin film systems during modulated laser heating," *J. Heat Transfer* **132**, 081302 (2010).
- ⁴⁰K. T. Regner, L. C. Wei, and J. A. Malen, "Interpretation of thermoreflectance measurements with a two-temperature model including non-surface heat deposition," *J. Appl. Phys.* **118**, 235101 (2015).
- ⁴¹K. T. Regner, J. P. Freedman, and J. A. Malen, "Advances in studying phonon mean free path dependent contributions to thermal conductivity," *Nanoscale Microscale Thermophys. Eng.* **19**, 183–205 (2015).
- ⁴²K. T. Regner, A. J. H. McGaughey, and J. A. Malen, "Analytical interpretation of nondiffusive phonon transport in thermoreflectance thermal conductivity measurements," *Phys. Rev. B* **90**, 064302 (2014).
- ⁴³K. T. Regner, D. P. Sellan, Z. Su, C. H. Amon, A. J. H. McGaughey, and J. A. Malen, "Broadband phonon mean free path contributions to thermal conductivity measured using frequency domain thermoreflectance," *Nat. Commun.* **4**, 1640 (2013).
- ⁴⁴A. T. Ramu and J. E. Bowers, "A compact heat transfer model based on an enhanced Fourier law for analysis of frequency-domain thermoreflectance experiments," *Appl. Phys. Lett.* **106**, 263102 (2015).
- ⁴⁵Y. K. Koh and D. G. Cahill, "Frequency dependence of the thermal conductivity of semiconductor alloys," *Phys. Rev. B* **76**, 075207 (2007).
- ⁴⁶Y. K. Koh, D. G. Cahill, and B. Sun, "Nonlocal theory for heat transport at high frequencies," *Phys. Rev. B* **90**, 205412 (2014).
- ⁴⁷R. Cheaito, J. C. Duda, T. E. Beechem, K. Hattar, J. F. Ihlefeld, D. L. Medlin, M. A. Rodríguez, M. J. Champion, E. S. Piekos, and P. E. Hopkins, "Experimental investigation of size effects on the thermal conductivity of silicon-germanium alloy thin films," *Phys. Rev. Lett.* **109**, 195901 (2012).
- ⁴⁸B. Abeles, "Lattice thermal conductivity of disordered semiconductor alloys at high temperatures," *Phys. Rev.* **131**, 1906–1911 (1963).
- ⁴⁹P. G. Klemens, "The scattering of low-frequency lattice waves by static imperfections," *Proc. Phys. Soc., London, Sect. A* **68**, 1113–1128 (1955).
- ⁵⁰P. E. Hopkins, "Dispersion considerations affecting phonon-mass impurity scattering rates," *AIP Adv.* **1**, 041705 (2011).